Impact of Claw-Pole Geometry Variations on the Performance of Machine used in Automotive Application

Pranshu Upadhayay[1,2], Afef Kedous-Lebouc[1], Lauric Garbuio[1]
[1]Univ. Grenoble Alpes, CNRS, Grenoble INP, G2Elab,
F-38000 Grenoble, France,
email: pranshulink@gmail.com

Jean-Claude Mipo[2], Jean-Marc Dubus[2]
[2]Valeo - Equipements Electriques Moteur
2 rue André Boulle
94000 Créteil, France

***Abstract* — This paper presents the influence of variation in various geometric parameters of claw-pole topology on the performance of machine used in automotive application. Due to three-dimensional flux distribution in the claw-pole topology, variation in geometric parameters of the claw-poles results into change in performance of the machine. The geometric parameters which have been varied are claw core outer diameter, claw inside radius, claw side plate thickness and claw undercut angle, and the performance of the machine has been evaluated for the complete operational speed range from low speed of 600 rpm to high speed of 18,000 rpm. By carrying out the aforesaid variations, it has been observed that there is a significant change in torque during low speed operation.**

Keywords — claw-pole, automotive, finite element, alternator, motor, permanent magnet

I. Introduction

In automotive applications, a machine topology that has garnered much research interest is the claw-pole topology which consists of a three-dimensional (3-D) flux path. With the increase in features of comfort, safety and luxury in automobiles, the power requirements for automotive applications are increasing day by day. Consequently, there is also a need of higher fuel efficiency and the automotive applications are moving towards higher voltages of 48 V from erstwhile 12V systems with increased output power requirements [1]. Generators of output power up to 5 kW and speeds up to 18,000 rpm for these applications are solely dominated, till date, by claw-pole type machines [2].

A conventional claw-pole machine consists of a 3-phase or multi-phase stator with windings and two forged claw-poles as rotor with ring shaped field coil, fed with direct current (DC) via slip rings and carbon brushes. The 3-D flux distribution in the claw-pole machine is due to its claw type rotor structure and hence requires 3-D finite element (FE) magnetic field analysis. Fig. 1 illustrates the geometry of a conventional claw-pole machine with its main flux path through the magnetic circuit and therefore we can observe the 3-D flux distribution [3]. Permanent magnets (PMs) due to their high energy density are increasing being used to increase and improve the power capabilities of electrical machines. Therefore, in a permanent magnet based claw-pole machine, the PMs are placed in the inter-claw region i.e. between the two claw poles, to provide increased magnetic flux and reduce flux leakage between the consequent claw poles [4].

Fig. 1. Main 3-D flux path in a conventional claw-pole machine [3]

Design optimization of claw-pole machine requires rigorous design iterations by geometric parameter variations. This result into huge time consuming optimization algorithms to be run in parallel to obtain appropriate results for the complete torque-speed curves. Therefore, this paper illustrates the effect of variation in geometric parameters of the claw-poles on the performance of the machine in the complete operational speed range of 600 rpm to 18,000 rpm and hence provides information that geometry optimization could only be concentrated in the constant torque region and not for the complete speed range. The different geometry parameters utilized for the study are claw core outer diameter, claw inside radius, claw side plate thickness and claw undercut angle. These parameters are varied within a specific range of minimum and maximum, taking the manufacturing and production design into consideration. It has been observed that there is a significant variation in torque during low speed operation with the alteration in the above stated geometric parameters of the claw-poles.

II. Geometric Parameters and Analysis Methodology Utilized in the Machine

Various techniques have been researched upon for analytical based design analysis of the claw-pole machine in different research papers. It is observed that preference lies in using lumped parameter or analytical based design approach

for initial design of the machine due to high computational time required for 3-D FE analysis. Magnetic equivalent circuit and reluctance network based design analysis has been investigated in literature [5]-[8], and the design results have promising agreement with experimental results, hence validating their design methodology. Therefore, these design methodologies can be used to quickly design an initial claw-pole machine for a particular specification and subsequently fine tuned for various geometric parameters using 3-D FE analysis, which is more accurate than analytical based design approach.

The claw-pole machine analyzed in this paper is based on claw-pole rotor with PMs placed in the inter-claw region. Fig. 2 (a) shows the cross sectional front view of the designed claw-pole machine and Fig. 2 (b) shows the sectional isometric view of the claw-poles, magnets and rotor winding.

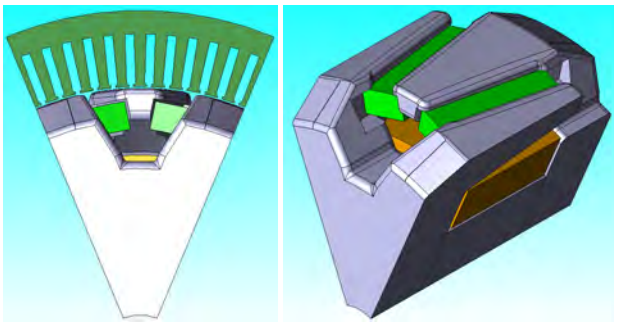

(a) (b)

Fig. 2. Cross-sectional views of the claw-pole machine (a) Front view of the machine (b) Isometric view of the claw-poles, magnets and rotor winding

The structure of the claw-poles is complex due to its asymmetrical geometry in the two-dimensional (2-D) plane and therefore requires additional modeling time to get the actual geometry developed in any analysis software as compared with 2-D planar geometries. Fig. 3 provides the details of various claw-pole geometry parameters utilized in the study i.e. claw core outer radius, claw inside radius, claw side plate thickness and claw undercut angle.

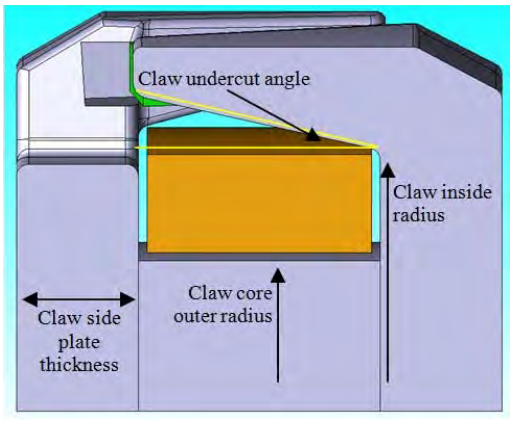

Fig. 3. Various geometric parameters of the claw-pole used for the study

The analysis methodology utilized for the machine has been carried out using classical electrical machine analysis theory using Park's transformation and later FE analysis has been investigated to evaluate the machine performance at various speeds [9]-[12]. The *dq* transformation equations utilized are as follows [9]:

$$\begin{bmatrix} F_d \\ F_q \\ F_0 \end{bmatrix} = \frac{2}{3}\begin{bmatrix} \cos\theta & \cos\left(\theta-\frac{2\pi}{3}\right) & \cos\left(\theta+\frac{2\pi}{3}\right) \\ -\sin\theta & -\sin\left(\theta-\frac{2\pi}{3}\right) & -\sin\left(\theta+\frac{2\pi}{3}\right) \\ \frac{1}{2} & \frac{1}{2} & \frac{1}{2} \end{bmatrix}\begin{bmatrix} F_a \\ F_b \\ F_c \end{bmatrix} \quad (1)$$

where, variable F can represent any of the following, i.e. electromotive force (EMF) e in volts, current (i) in Amps and flux linkage (ψ) in Wb. The θ is angular displacement of the rotor d-axis w.r.t. the a-phase.

The voltage equations are as follows:

$$V_d = R_s i_d + \frac{d\psi_d}{dt} - \omega\psi_q \quad (2)$$

$$V_q = R_s i_q + \frac{d\psi_q}{dt} + \omega\psi_d \quad (3)$$

where, V is the voltage in volts, R_s is the stator phase resistance in ohms and ω is the speed in rad/s.

Finally the torque in Nm is as below:

$$T = \frac{m}{2}P\left(\psi_d i_q - \psi_q i_d\right) \quad (4)$$

where, m is the no. of phases and P is the pole pair.

III. Effect of Geometric Parameter Variation

The study in this paper is mainly concentrated on 48 V mild-hybrid automotive applications, where the conventional starter motor and alternator are replaced by a belt-driven integrated motor-generator set generally known as integrated belt starter-generator [13]. As the main functions of integrated belt starter-generator are (a) to start the internal combustion engine (ICE) by running as inverter driven motor and (b) generating electric power during generator mode by controlled rectification through the inverter; therefore, the low speed operation during motoring mode is important as the machine needs to provide an adequate starting torque to crank the ICE during initial starting. Along-with the importance of low speed operation, there is also a need to evaluate the performance of the machine in constant power region, to verify the machine's capability to deliver sufficient power at higher speeds. The design study for peak output power of the machine in motoring mode has been carried out for the entire speed range to obtain torque vs. speed and power vs. speed curves. Therefore, the performance analysis is carried out for the following two investigations: (i) at low speed operation of 600 rpm and (ii) at complete speed range from 600 rpm to 18,000 rpm.

One of the major challenges in automotive applications is having minimum size and weight of the machine albeit with improved or increased performance. This makes it necessary to have manufacturing and production related design into consideration during parameterization and optimization of the machine. Hence, geometric parameters of the claw-poles are varied within a specific range of minimum and maximum, i.e. claw core outer radius is varied from 24 mm to 33 mm, claw inside radius is varied from 37 mm to 45 mm, claw side plate thickness is varied from 11 mm to 19 mm and claw undercut angle is varied from 10° to 18°.

A. At low speed operation (600rpm)

Torque at low speed of 600 rpm is evaluated for all the geometric parameter variations, which are as below:

1) Claw core outer radius:

The claw core outer radius is varied from 24 mm to 33 mm, thereby modifying claw core area and rotor winding area. With the increase in claw core outer radius, there is reduction in rotor winding area. The number of turns of the rotor winding has to be suitably designed so as to maintain approximately constant current density in the rotor winding while also maintaining about 80% rotor winding slot fill factor. As a result, in this case the number of turns of the rotor winding is varied so as to maintain approximately 11.6 AT/mm^2 as the current density in the rotor winding.

Fig. 4 shows the flux density plot of the machine with claw core outer radius at 24 mm and 33 mm respectively. It is observed that the claw core is highly saturated at 24 mm as compared to 33 mm with the same maximum scale of 2.2 T for the flux density value. Fig. 5 illustrates the variation of torque with change in claw core outer radius, and it can be observed that the torque increases initially from 24 mm to 30 mm and then decreases rapidly till 33 mm. The initial increase of torque is mainly due to reduction of claw core saturation till 30 mm and there after the claw core is totally unsaturated. However, the effective ampere-turns in rotor winding are reduced due to less availability of rotor winding area; in turn less amount of flux generation is possible through the claw core.

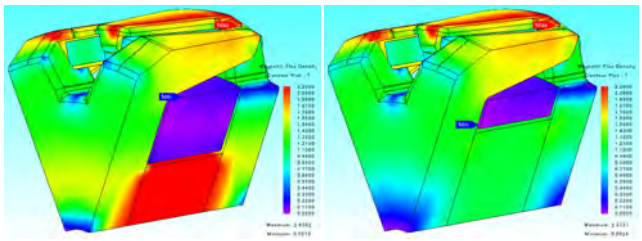

Fig. 4. Flux density plot of the machine with 24 mm and 33 mm as the claw core outer radius respectively

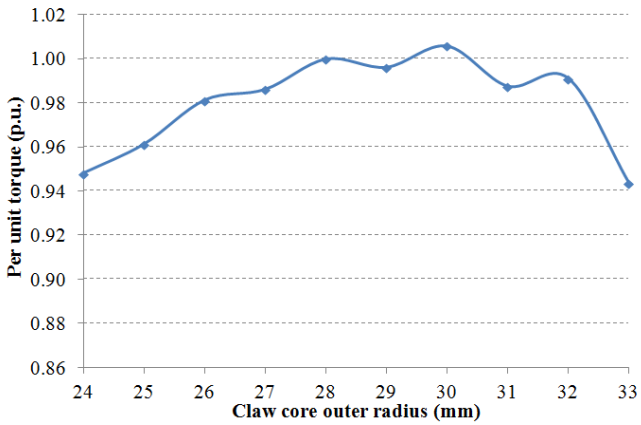

Fig. 5. Variation of torque with change in claw core outer radius

2) Claw inside radius:

The claw inside radius is varied from 37 mm to 45 mm, therefore modifying the rotor winding area. With the increase in claw inside radius, there is an increment in rotor winding area. The number of turns of rotor winding has to be appropriately designed in the same way as discussed in the previous section III, sub-section (1). In this study also the current density in the rotor winding is maintained at approximately 11.6 AT/mm^2.

Fig. 6 shows the flux density plot of the machine with claw inside radius at 37 mm and 45 mm respectively. It is observed that the claw core saturation changes slightly from 37 mm to 45 mm as compared to the saturation on the claw fingers which increases drastically from 37 mm to 45 mm for the same maximum scale of 2.2 T of flux density value. Fig. 7 illustrates the variation of torque with change in claw inside radius, and it can be observed that the torque increases from 37 mm to 42 mm and then decreases till 45 mm. The initial increase of torque is mainly due to unsaturated claw fingers till 42 mm and thereafter they are totally saturated in-spite of increase in the effective ampere-turns in rotor winding, therefore, flux increment in the air gap is restricted due to saturation of claw fingers.

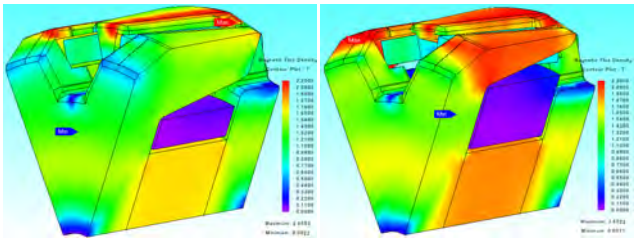

Fig. 6. Flux density plot of the machine with 37 mm and 45 mm as the claw inside radius respectively

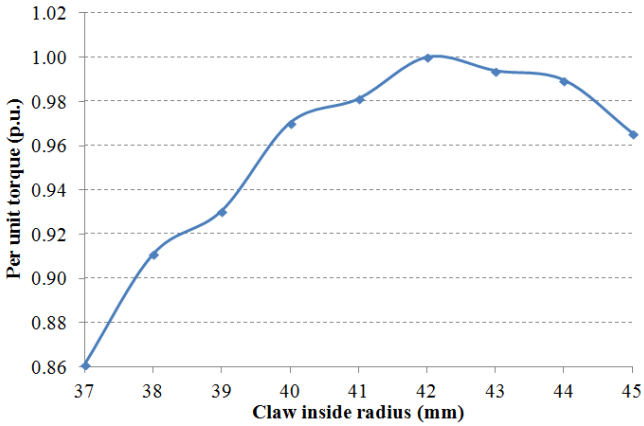

Fig. 7. Variation of torque with change in claw inside radius

3) Claw side plate thickness:

The claw side plate thickness is varied from 11 mm to 19 mm, hence modifying the side plate area and not altering the rotor winding area.

Fig. 8 shows the flux density plot of the machine with claw side plate thickness at 11 mm and 19 mm respectively. It is observed that the claw side plates are less saturated at 11 mm thickness as compared to at 19 mm thickness where they are totally unsaturated. It is also observed that the claw core is unsaturated at 11 mm thickness and it gets saturated at 19 mm thickness. Fig. 9 illustrates the variation of torque with change

in claw side plate thickness, and it can be observed that the torque increases from 11 mm to 19 mm thickness. The gradient of increment is more from 11 mm till 14 mm thickness in contrast to thickness from 14 mm till 19 mm and this is due to the start of saturation of claw core with the increase in claw side plate thickness.

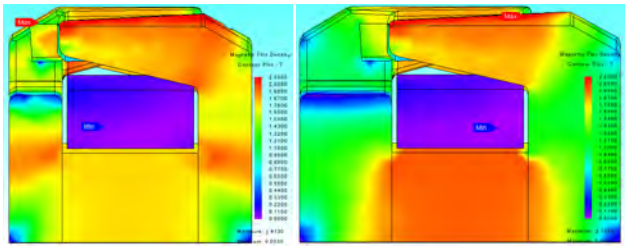

Fig. 8. Flux density plot of the machine with 11 mm and 19 mm as the claw side plate thickness respectively

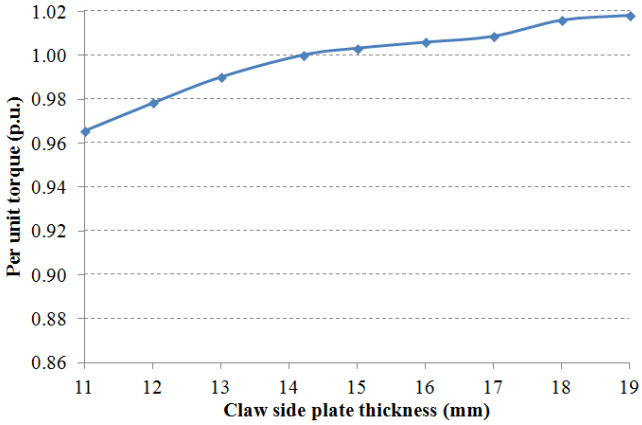

Fig. 9. Variation of torque with change in claw side plate thickness

4) Claw undercut angle:

The claw undercut angle is varied from 10° to 18°, hence modifying the claw finger area and not altering the rotor winding area.

Fig. 10 shows the flux density plot of the machine with claw undercut angle at 10° and 18° respectively and it is observed that there is small deviation in the flux density level of claw core area as well as in claw finger area. Fig. 11 illustrates the variation of torque with change in claw undercut angle and it can be observed that there is only slight modification in torque from 10° to 18°, and it is mainly due to the little variation in flux at claw core, claw fingers and air gap areas.

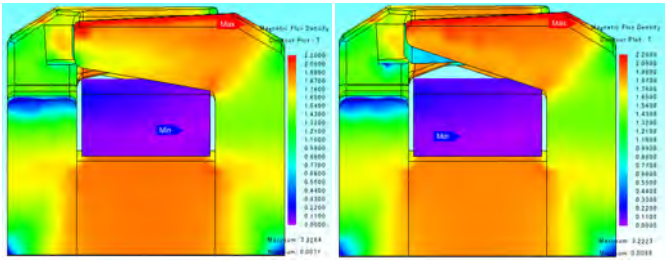

Fig. 10. Flux density plot of the machine with 10° and 18° as the claw undercut angle respectively

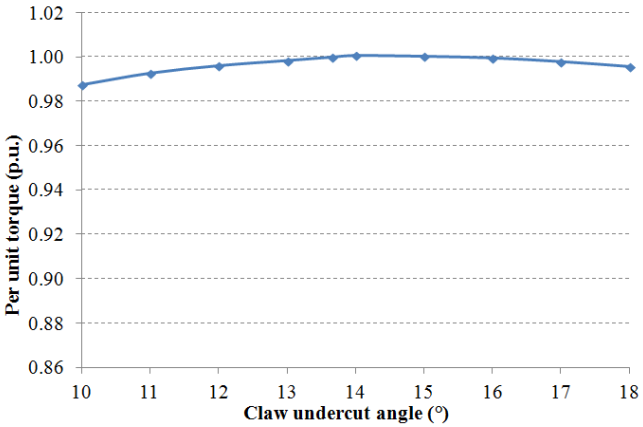

Fig. 11. Variation of torque with change in claw undercut angle

Consequently, we can observe from the aforementioned four cases that with the variation of geometric parameters, there is alteration in torque of the machine at low speed. To quantify the above analysis, percentage change in torque is calculated for all the aforesaid cases in the following way:

$$T_{avg} = \frac{T_{max} + T_{min}}{2} \quad (4)$$

$$\%T = \frac{(T_{max} - T_{\min}) * 100}{T_{avg}} \quad (5)$$

where for each case, T_{max} and T_{min} are the per unit (p.u.) maximum and minimum torque, T_{avg} is average p.u. torque which is calculated by (4), and $\%T$ is percentage change in torque which is calculated by (5). Table I shows T_{max}, T_{min}, T_{avg} and $\%T$ for all the geometric parameters and it can be observed that for claw core outer radius, claw inside radius, and claw side plate thickness the $\%T$ varies from 5% to 15% which is a significant value.

TABLE I. TMAX, TMIN, TAVG AND %T FOR ALL THE GEOMETRIC PARAMETERS

Geometric Parameter	Tmax (p.u.)	Tmin (p.u.)	Tavg (p.u.)	%T (%)
Claw core outer radius	1.006	0.944	0.975	6.38
Claw inside radius	1.000	0.861	0.931	14.92
Claw side plate thickness	1.018	0.965	0.992	5.30
Claw undercut angle	1.001	0.988	0.994	1.32

B. At complete speed range operation (600 to 18,000 rpm)

To obtain the complete torque vs. speed and power vs. speed curves for the claw-pole machine, it is very important to optimize the stator current, field current and current angle, so as to obtain the constant torque and power region without exceeding the voltage limit of 48 V DC.

Multi-objective genetic algorithm methodology was adopted for performance evaluation in the complete speed range. The objective functions in this analysis were (i) to maximize the torque and (ii) to limit the voltage at 48 V DC. The FE models of all the geometric variations were realized and performance parameters were evaluated at various speeds, which are as below:

1) Claw core outer radius:

Fig. 12 and Fig. 13 illustrate the torque vs. speed and power vs. speed curves in p.u. with change in claw core outer radius. It can be observed that the modification of torque is higher in constant torque region as compared to the constant power region.

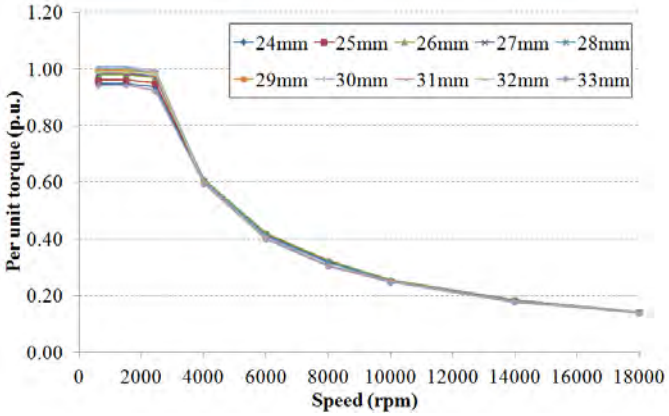

Fig. 12. Torque vs. speed with change in claw core outer radius

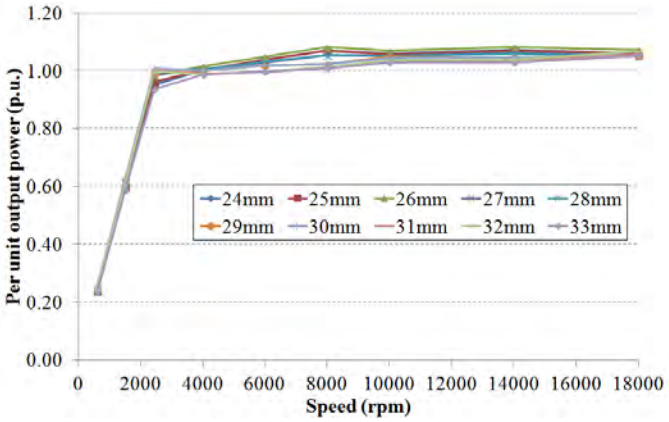

Fig. 13. Power vs. speed with change in claw core outer radius

2) Claw inside radius:

Fig. 14 and Fig. 15 illustrate the torque vs. speed and power vs. speed curves in p.u. with change in claw inside radius. It can also be observed that the change in torque is larger in constant torque region as compared to the constant power region, comparatively similar to previous case of claw core outer radius parameter.

3) Claw side plate thickness:

Fig. 16 and Fig. 17 illustrate the torque vs. speed and power vs. speed curves in p.u. with change in claw side plate thickness. It can again be observed that the variation of torque is greater in constant torque region as compared to the constant power region, rather similar to previous two cases of claw core outer radius and claw inside radius parameters.

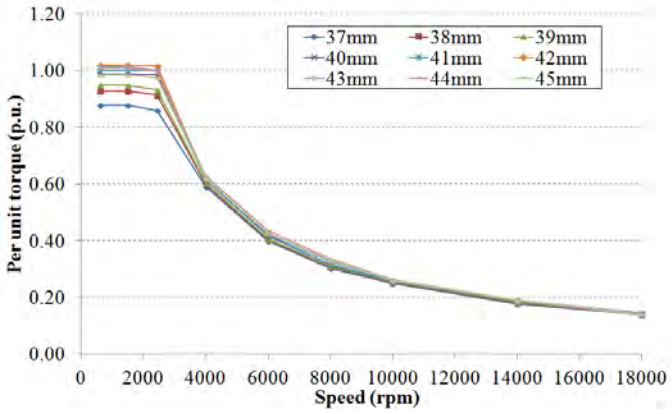

Fig. 14. Torque vs. speed with change in claw inside radius

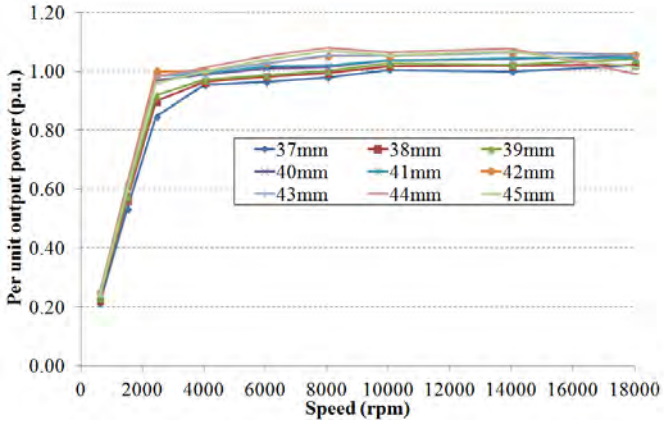

Fig. 15. Power vs. speed with change in claw inside radius

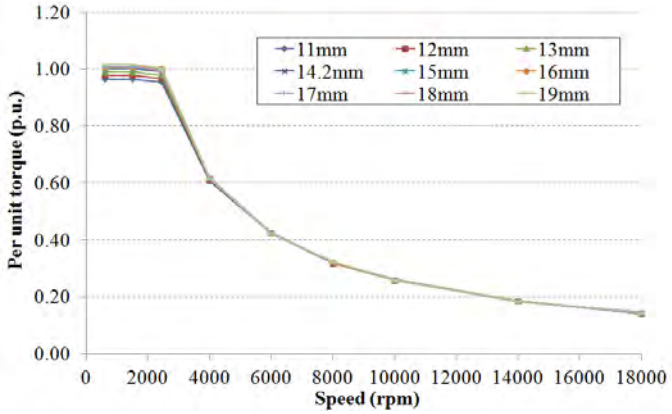

Fig. 16. Torque vs. speed with change in claw side plate thickness

4) Claw undercut angle:

Fig. 18 and Fig. 19 illustrate the torque vs. speed and power vs. speed curves in p.u. with change in claw undercut angle. It can be observed that in both the constant torque and constant power region there is almost no alteration in torque and power for the entire speed range.

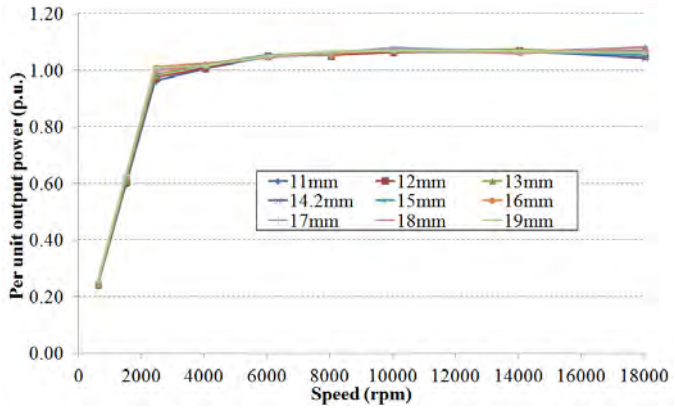

Fig. 17. Power vs. speed with change in claw side plate thickness

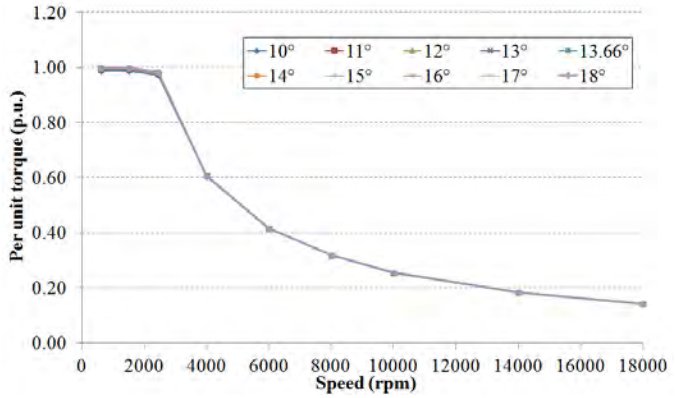

Fig. 18. Torque vs. speed with change in claw undercut angle

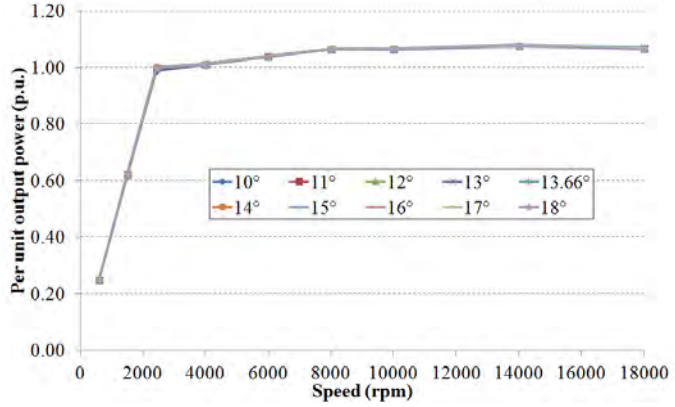

Fig. 19. Power vs. speed with change in claw undercut angle

As a result we can observe from the above four cases that with variation of above geometric parameters, there is consequent modification of torque in constant torque region, thereby emphasizing on performing geometry optimization at low speeds rather than in complete speed range as a scope of future work.

IV. Conclusion

In this paper, the torque at low speed operation of 600 rpm varies from 5 to 15% with change in geometric parameters of the claw-pole machine. This is predominantly due to change in reluctance of geometric parameters, consequently affecting the flux throughout the machine. The torque vs. speed and power vs. speed curves for the complete speed range shows that significant change in torque occurs in constant torque region whereas there is almost no alteration of torque in constant power or field weakening region. It can thus be concluded that geometry optimization of the claw-pole machine can fully be concentrated in the low speed range, and verification of performance can be carried out for the complete speed range after optimization convergence.

Acknowledgement

The research leading to these results has received funding from European Community's Horizon 2020 Programme ([H2020/2014-2019)] under Grant Agreement no. 674973 (MSCA-ETN DEMETER). This publication reflects only the author's view, exempting the Community from any liability. Project website: http://etn-demeter.eu/.

References

[1] I. G. Kassakian, H.-C. Wolf, J. M. Miller, and C.J. Hurton, "Automotive electrical systems circa 2005", IEEE Spectrum, 33, 8, August, 1996.

[2] Ion Boldea, "Variable Speed Generators", CRC Press, Taylor & Francis Group, 2006, pp. 6-1 – 6-34.

[3] A. Ibala, R. Rebhi and A. Masmoudi, "MEC-Based Modelling of Claw Pole Machines: Application to Automotive and Wind Generating Systems", International Journal of Renewable Energy Research, IJRER, vol. 1, no. 3, pp.1-8, 2011.

[4] L. Tutelea, D. Ursu, I. Boldea and S. Agarlita, "IPM Claw-Pole Alternator System for more Vehicle Braking Energy Recuperation", Journal of Electrical Engineering, vol. 12, no. 3, pp. 211-220, 2012.

[5] V. Ostovic, J. M. Miller, V. K. Garg, R. D. Schultz and S. H. Swales, "A Magnetic-Equivalent-Circuit-Based Performance Computation of a Lundell Alternator", IEEE Transactions on Industry Applications, vol. 35, no. 4, pp. 825-830, July/August 1999.

[6] Sang-Ho Lee, Soon-O. Kwon, Jeong-Jong Lee, and Jung-Pyo Hong, "Characteristic Analysis of Claw-Pole Machine Using Improved Equivalent Magnetic Circuit", IEEE Transactions on Magnetics, vol. 45, no. 10, pp. 4570-4573, October 2009.

[7] L. Albert, C. Chillet, A. Jarosz, J. Rousseau and F. Wurtz, "Sizing of automotive claw-pole alternator based on analytical modeling", Electromotion, 2005, 12 (5/6), pp.749-772.

[8] A. Delale, L. Albert, L. Gerbaud and F. Wurtz, "Automatic Generation of Sizing Models for the Optimization of Electromagnetic Devices Using Reluctance Networks", IEEE Transactions on Magnetics, vol. 40, no. 2, pp. 830-833, March 2004.

[9] R. H. Park, "Two Reaction Theory of Synchronous Machines: Generalized Method of Analysis-Part I", Transactions of the American Institute of Electrical Engineers, vol. 48, no. 3, pp. 716-727, July 1929.

[10] G. Henneberger, S. Kuppers and I. Ramesohl, "Numerical Calculation, Simulation and Design Optimisation of Claw Pole Alternators for Automotive Application", IEE Colloquium on Machines for Automotive Applications (Digest No. 1996/166), pp. 3/1-3/5, November 1996.

[11] C. Stoica, L. M. Constantinescu, E. Lefter and B. Enache, "Computation of the Characteristics of a Claw Pole Alternator through the Finite Element Method", 2013 International Conference on Electronics, Computers and Artificial Intelligence (ECAI), pp. 1-4, June 2013.

[12] P. Upadhayay, A. Kedous-Lebouc, L. Garbuio, J. C. Mipo, J. M. Dubus, "Design & Comparison of a Conventional and Permanent Magnet based Claw-Pole Machine for Automotive Application", 15th International Conference on Electrical Machines, Drives and Power Systems (ELMA 2017), pp. 1-5, June 2017.

[13] I. A. Viorel, L. Szabó, L. Löwenstein and C. Stet, "Integrated Starter-Generators For Automotive Applications", Acta Electrotehnica, vol. 45, no. 3, pp. 255–260, 2004.